A Fully Explicit Wave-Vegetation Interaction Model and Its Application in Waves over a Floating Seaweed Farm

Zhilong Wei[a,b], **Yanlin Shao**[a,*], **Trygve Kristiansen**[b], **David Kristiansen**[b]

a. Department of Civil and Mechanical Engineering, Technical University of Denmark, 2800, Lyngby, Denmark

b. Department of Marine Technology, Norwegian University of Science and Technology, NO-7491, Trondheim, Norway

*Corresponding author. Email: yshao@dtu.dk

1 Introduction

A fully explicit coupled wave-vegetation interaction model has been developed to efficiently solve the coupled wave dynamics and flexible vegetation motion with large deflections. The flow model is formulated using the continuity equation and linearized momentum equations of an incompressible flow, with additional terms within the canopy region accounting for the presence of vegetation. A second-order unconditionally stable explicit scheme is developed to solve the linearized flow model. A truss-spring model is proposed to capture the vegetation motion with substantial deflections, allowing for explicit time integration with large time steps when dealing with highly compliant vegetation. The coupled model is first validated against experiments on the reconfiguration of an elastic blade in oscillatory flow and then employed to investigate wave propagation over a floating seaweed farm, demonstrating its efficiency and robustness in addressing wave-vegetation interaction problems.

2 Theory

The continuity equation and linearized momentum equations of an incompressible flow have been widely used in the derivation of analytical solutions for wave attenuation over permeable media, which inspired us to develop a linearized numerical flow solver. As demonstrated in Fig. 1, additional terms are added to the linearized momentum equation within the canopy region, accounting for the drag and inertia loads on the vegetation.

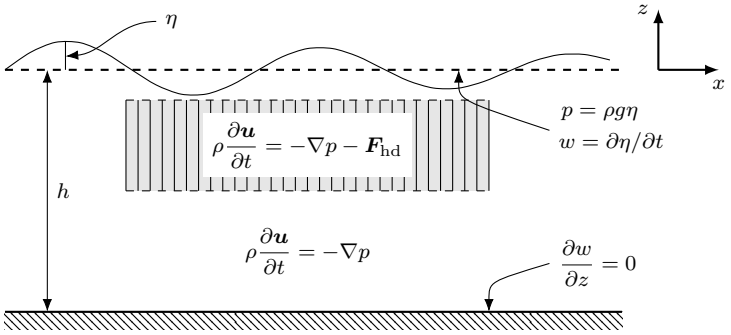

Figure 1: Definitions in the linearized flow solver. Inside the vegetation region (shaded area), an extra source term due to the presence of vegetation, $\boldsymbol{F}_{\mathrm{hd}}$, is added to the linearized momentum equation to account for the presence of the vegetation. $\boldsymbol{u}$ is the flow velocity, p is the dynamic pressure, and η is the free-surface elevation. t denotes time.

The general governing equation of motion for a compliant blade is

$$\mu\frac{\partial^2 \boldsymbol{r}}{\partial t^2} - EA\frac{\partial}{\partial s}\left[\left(1-\left(\frac{\partial \boldsymbol{r}}{\partial s_0}\cdot\frac{\partial \boldsymbol{r}}{\partial s_0}\right)^{-1/2}\right)\frac{\partial \boldsymbol{r}}{\partial s_0}\right] + EI\left[\frac{\partial^4 \boldsymbol{r}}{\partial s^4} - \frac{\partial}{\partial s}\left(\left(\frac{\partial \boldsymbol{r}}{\partial s}\cdot\frac{\partial^3 \boldsymbol{r}}{\partial s^3}\right)\frac{\partial \boldsymbol{r}}{\partial s}\right)\right] = \boldsymbol{q}, \tag{1}$$

where s_0 and s are the unstretched and stretched arc length along the blade, $\boldsymbol{r}$ is the position vector of a point on the blade, $\boldsymbol{q}$ is the external distributed load, A and I are the instant cross-section area and second moment of area, μ is the instant mass per unit length, and E is Young's modulus. t denotes time.

The external distributed load $\boldsymbol{q}$ includes gravity, buoyancy, and hydrodynamic forces. Following [1], the distributed hydrodynamic load on the body consists of two parts, the resistive drag $\boldsymbol{q_d}$ and the reactive force $\boldsymbol{q_{am}}$

$$\boldsymbol{q_d} = -\frac{1}{2}\rho C_D b|U_n|U_n\boldsymbol{n}, \quad \boldsymbol{q_{am}} = -m_a\left(\frac{\partial(U_n\boldsymbol{n})}{\partial t} - \frac{\partial(U_\tau U_n\boldsymbol{n})}{\partial s} + \frac{1}{2}\frac{\partial(U_n^2\boldsymbol{\tau})}{\partial s}\right), \tag{2}$$

where U_n and U_τ are the normal and tangential components of the relative velocity between the blade and the ambient flow, i.e. $U_n\boldsymbol{n} + U_\tau\boldsymbol{\tau} = \partial\boldsymbol{r}/\partial t - \boldsymbol{U}$. $m_a = \pi\rho b^2/4$ is the added mass, b is the cross-section span of the blade, and C_D is the drag coefficient. $\boldsymbol{n}$ and $\boldsymbol{\tau}$ are respectively the blade tangential vector and normal vector.

For some aquaculture vegetation, such as seaweed, since the blade can be thin and the density of vegetation is close to water, the added mass is much larger than the body mass. If an explicit time-integration method is applied to solve Eq. (1), the solution will be unstable. Therefore, Eq. (1) has been re-formulated so that the added-mass terms associated with the local structural acceleration are explicitly separated from other reactive-force terms and moved to the left-hand side of the equation, leading to an alternative form, which is ready to be solved by standard explicit schemes. Meanwhile, as the strain is usually small for marine vegetation, it is a good approximation to assume that the vegetation is inextensible to further simplify the hydrodynamic loads. To this end, we have derived the following alternative form of the governing equation of motion for a flexible blade or stem

$$\begin{aligned}(\mu\boldsymbol{I} + m_a\boldsymbol{n}\boldsymbol{n}^T)\frac{\partial^2\boldsymbol{r}}{\partial t^2} &\overbrace{-EA\frac{\partial}{\partial s}\left[\left(1-\left(\frac{\partial\boldsymbol{r}}{\partial s_0}\cdot\frac{\partial\boldsymbol{r}}{\partial s_0}\right)^{-1/2}\right)\frac{\partial\boldsymbol{r}}{\partial s_0}\right]}^{\text{tension}} + \overbrace{EI\left[\frac{\partial^4\boldsymbol{r}}{\partial s^4} - \frac{\partial}{\partial s}\left(\left(\frac{\partial\boldsymbol{r}}{\partial s}\cdot\frac{\partial^3\boldsymbol{r}}{\partial s^3}\right)\frac{\partial\boldsymbol{r}}{\partial s}\right)\right]}^{\text{bending moment}} \\ &= -\frac{1}{2}\rho C_D b|U_n|U_n\boldsymbol{n} + m_a\left(\frac{\partial\boldsymbol{U}}{\partial t}\cdot\boldsymbol{n}\right)\boldsymbol{n} + 2m_aU_\tau\frac{\partial^2\boldsymbol{r}}{\partial s\partial t} - m_a\left(U_\tau^2 - \frac{1}{2}U_n^2\right)\frac{\partial^2\boldsymbol{r}}{\partial s^2} \\ &\quad - m_a\left(\left(\frac{\partial\boldsymbol{U}}{\partial s}\cdot\boldsymbol{\tau}\right)U_n + \left(\frac{\partial\boldsymbol{U}}{\partial s}\cdot\boldsymbol{n}\right)U_\tau\right)\boldsymbol{n} + m_aU_n\left(\frac{\partial\boldsymbol{U}}{\partial s}\cdot\boldsymbol{n}\right)\boldsymbol{\tau} + \boldsymbol{G} + \boldsymbol{B},\end{aligned} \tag{3}$$

where $\boldsymbol{G}$ and $\boldsymbol{B}$ are gravity and buoyancy components. $\boldsymbol{I}$ is an identity matrix. The term $m_a\boldsymbol{n}\boldsymbol{n}^T$ changes with the blade position and behaves as an *generalized added mass*. For a rigid structure, this term will reduce to $m_a\boldsymbol{I}$.

3 Numerical Methods

The flow motion, governed by the continuity equation and linearized momentum equations, is solved in the time domain based on a second-order finite difference method. The projection method is adopted to maintain a divergence-free velocity field. It can be shown that the numerical flow solver is unconditionally stable.

We have also developed a *truss-spring model* to model the large-amplitude deformation of compliant vegetation. The flexible vegetation blade is represented by end-to-end trusses, as shown in Fig. 2a. The second term and the third term on the left-hand side of Eq. (3), respectively, represent tension and bending moment. The tension is given explicitly according to Hooke's law. A massless rotation spring is added to each node to model the bending stiffness. Since lumped masses are used in the truss model to take into account the inertia of the structure, it is not straightforward to apply a moment on the nodes to account for bending moments. To address this, we introduce an equivalent couple at the two nodes of each truss to represent the bending moment. It can be proven that the present truss-spring model is mathematically consistent with the governing equations Eq. (3).

The coupling of the waves and the flexible structure motion loosely follows the immersed boundary method. The general idea is that the hydrodynamic force acting on the structure by the fluid is integrated over the adjacent region (shaded area in Fig. 2b) weighted by a modified Dirac delta function, and vice versa for the force acting on the fluid by the structure.

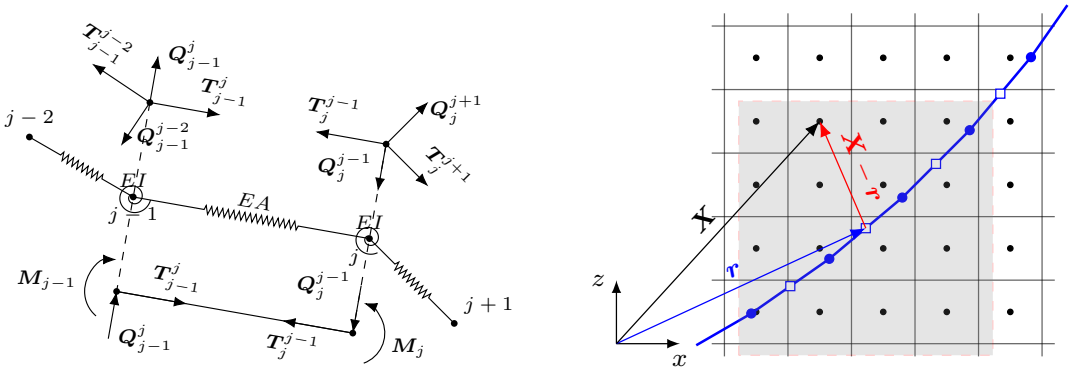

(a) Truss-spring model (b) Immersed boundary method

Figure 2: (a) Tensions and moments on a truss element; tensions and the couples on the nodes. (b) A Lagrangian structure grid (blue curve) immersed in the background Eulerian fluid grid (black mesh).

The critical time step for the explicit truss-spring model is given by $\Delta l/c_s$, where Δl is the minimum length of the truss elements, $c_s = \sqrt{E/\rho_s}$ is the sound speed in the structure material, and E and ρ_s are the Young's modulus and density of the structure material. It is evident that a smaller E, indicative of a more flexible material, allows for a larger critical time step size. Thus the truss-spring model exhibits greater efficiency when applied to softer materials.

4 Results

The reconfiguration of elastic blades in oscillatory flow has been investigated both experimentally and numerically in [1]. We define KC $= 2\pi A/l_0$ in terms of the blade initial length l_0 to describe the problem, in which A is the amplitude of the oscillation flow. The experiments were carried out only at small KC values. For KC $= 1.7$ and 4.1 where experimental results are available, our predicted tip trajectories of the blade agree very well with both the numerical results and experiments from [1], as demonstrated in Fig. 3 (a) and (b). The structure model used in [1], a pseudo-Newton solver with an implicit time-stepping scheme, is rather different from the present truss-spring model, but our numerical results agree almost perfectly with theirs. The fact that both models have used the same load model described in Section 2 may explain this. Note that both numerical models give symmetrical results, while the experimental measurements are slightly shifted to the right. As illustrated in Fig. 3 (c), at much higher KC (exemplified with KC $= 62.8$), the blade will switch sides very fast (few snapshots visible in the middle but many are superimposed on the sides) and fluttering happens during the long period of quasi-static adaption following a fast reversal.

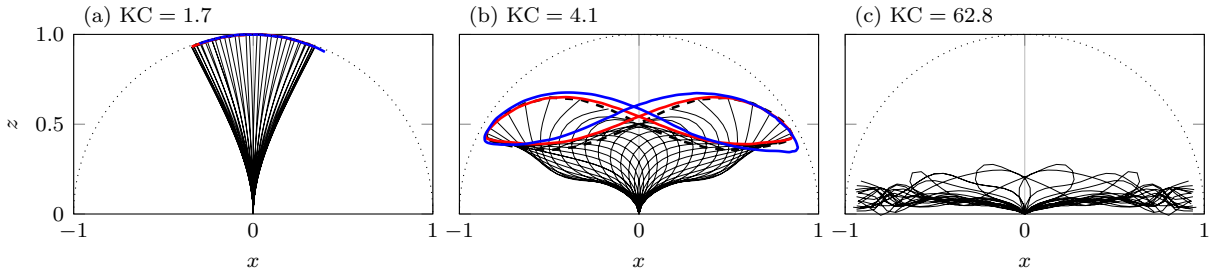

Figure 3: Comparison of the tip trajectory for two cases at different KC numbers. The blue curve and the red curve are the experimental measurements and numerical results from [1]; the dashed black curves represent the present results. 40 snapshots from the present model with a constant time interval over one period are presented as well. $C_D = 2$ for all cases, the same as applied in [1]. The blade was discretized into 20 truss elements. (a) KC $= 1.7$; (b) KC $= 4.1$; (c) KC $= 62.8$.

We also use the coupled model to study the waves over a floating seaweed farm located in a sheltered area of the Koster archipelago, Sweden [2]. The seaweed farm consists of 26 parallel

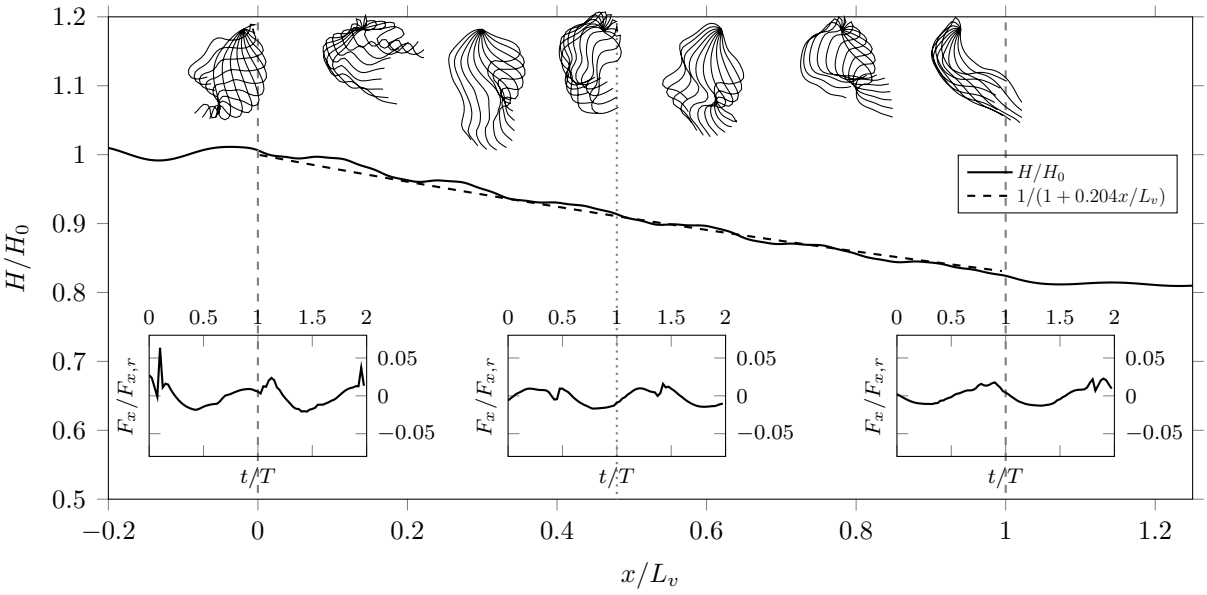

Figure 4: Wave attenuation over a seaweed farm, 11 snapshots of the blade trajectory within one period for blades located at $x = \{0, 16, 32, 48, 64, 80, 96\}$ m, and the total horizontal loads on the blade during 40th–42nd periods, normalized by the horizontal load on a rigid blade with the same geometry, for blades located at $x = \{0, 48, 100\}$ m. Wave period $T = 5\,\mathrm{s}$, incident wave height $H_0 = 1.5\,\mathrm{m}$, wavelength $\lambda = 36.6\,\mathrm{m}$. Seaweed farm span $L_v = 2.7\lambda = 100\,\mathrm{m}$.

longlines with an interval of 4 m. The longlines are submerged 2 m beneath the water surface. The seaweed blades ($\rho = 1230\,\mathrm{kg/m^3}$, $E = 5.6\,\mathrm{MPa}$), averagely $1.5\,\mathrm{m} \times 10\,\mathrm{cm} \times 2\,\mathrm{mm}$ by harvest season, are suspended on the longlines. The number of blades per meter along the longline is 120. We assume that the waves propagate perpendicular to the longlines and the problem can be simplified into 2D. In this case, we set $C_D = 2.0$.

The length of the computational domain was 8 times the wavelength. A uniform grid was used in the flow solver, with 80 grid points per wavelength and 60 grid points in the vertical direction over the water depth. In the structural solver, each stem was discretized into 30 truss elements. It took 898 s to run this case on a single 2.60 GHz CPU to simulate this case for 42 wave periods.

Given incident wave height $H_0 = 1.5\,\mathrm{m}$, wave period $T = 5\,\mathrm{s}$, and water depth $h = 10\,\mathrm{m}$, the wave transmission ratio is around 0.81. Even though the seaweed is flexible and the canopy is not uniformly distributed in the horizontal plane, the classic wave-attenuation theory based on energy conservation can be used to fit the wave decay. As shown in Fig. 4, the fitted wave heights $H/H_0 = 1/(1 + 0.204x/L_v)$ agree quite well with the present numerical results, where $L_v = 100\,\mathrm{m}$ is the span of the seaweed farm in the wave propagation direction.

Due to high flexibility, the motion of the seaweed blades and the load on the seaweed are non-periodic. The previously observed anti-symmetric behavior of more rigid blades in waves is also evident here. The antisymmetry is so significant that the blade will roll over the pinned top. Peaks in the total horizontal load on the blades were observed as well. The truss-spring model is robust enough to capture such features. More results will be presented in the workshop. This work was partly supported by the Research Council of Norway through SFI BLUES, grant number 309281.

References

[1] Leclercq, T. and de Langre, E. [2018], 'Reconfiguration of elastic blades in oscillatory flow', *Journal of Fluid Mechanics* **838**, 606–630.

[2] Thomas, J. B. E., Sodré Ribeiro, M., Potting, J., Cervin, G., Nylund, G. M., Olsson, J., Albers, E., Undeland, I., Pavia, H. and Gröndahl, F. [2021], 'A comparative environmental life cycle assessment of hatchery, cultivation, and preservation of the kelp Saccharina latissima', *ICES Journal of Marine Science* **78**(1), 451–467.